Journal of Applied Physics

AIP Publishing

Investigation of time variations of redox reactions in $SrRuO_3$ through interface-sensitive resistance measurements

Hiroshi Kambara,[a)] Hiroshi Shimazaki, and Kenichi Tenya

Department of Physics, Faculty of Education, Shinshu University, Nagano 380-8544, Japan

(Dated: 11 March 2023)

We used an interface-sensitive resistance measurement technique to observe the time evolution of the early stages of redox reactions at the interface between the metallic oxide $SrRuO_3$ and a silver epoxy electrode at around room temperature ($\sim 280-320$ K). On exposure to a reducing gas (CO or H_2), the interface resistance gradually increased. The time variation functions of the resistance increases for CO and H_2 were similar, although the magnitude was greater for H_2 than for CO. After substitution of O_2 for the reducing gas, the interface resistance decreased to almost the initial value, i.e., that before exposure to a reducing gas. The resistance variations can be well explained by the time variations of the oxygen deficiency at the $SrRuO_3$ interface and subsurfaces as a result of reduction or oxidation. We regarded the reactions as pseudo-first-order reactions, and evaluated the rate constants of the $SrRuO_3$ redox reactions at a $SrRuO_3$-Ag interface. For the reduction (resistance increase) process, a single exponential component was enough to fit the data, which suggests the reduction proceeds successively from outside to inside the bulk. Adsorption of oxygen atoms in the oxidation (resistance decrease) process involved several rate constants, at least up to three exponential components, depending on the prior degradation by a reducing gas. The effective activation energy of each redox reaction was evaluated from an Arrhenius plot.

[a)]kambara@shinshu-u.ac.jp

I. INTRODUCTION

Conducting oxide materials are stable in air at ambient pressure. At room temperature, common oxides are not reduced, even in a reducing environment, because the temperature is too low. However, raising the temperature usually accelerates reduction and finally leads to decomposition[1]. Recently, we used interface-sensitive resistance measurements to observe the slow reducing reactions that occurred at a polycrystalline $SrRuO_3$ (SRO)-metal interface in a hydrogenous environment at a relatively low temperature (room temperature)[2].

SRO is a stoichiometric conducting oxide with an undoped pseudocubic perovskite structure[3,4]. Because of its high electrical conductivity and good lattice matching with other perovskite materials, SRO is used as an electrode in functional oxide devices[4]. However, SRO annealing in forming gas (which contains H_2) causes degradation as a result of oxygen deficiency[5–10]. In most cases, annealing temperatures are higher than $200 - 300$ °C. Our previous work[2] showed that in hydrogenous environments surface/interface reactions occur even at room temperature, at which bulk reactions do not occur.

In this study, we used a three-terminal resistance method to investigate time variations of increases in the SRO-Ag interface resistance on exposure to a reducing gas, i.e., H_2 or CO, at room temperature[2]. We also investigated the time variations of decreases in the SRO-Ag interface resistance after substitution of O_2 for the reducing gas. These interface resistance variations can be understood in terms of oxygen deficiency at the SRO-Ag interface and at the SRO-Ag subsurfaces. Although room temperature is too low for bulk redox reactions, such reactions proceed slowly at a surface/interface at room temperature, and can therefore be used to follow the time variations of redox reactions with high accuracy by using a simple resistance measurement technique.

II. EXPERIMENTAL METHODS

Polycrystalline SRO samples were prepared by using a conventional solid-state reaction method. After careful mixing of $SrCO_3$ and RuO_2 powders, the mixed materials were shaped into pellets and sintered at 1050 °C in air at ambient pressure. The pellets were crushed, and the sintering process was repeated with an O_2 gas flow. Scanning electron microscopy observations showed that the grain size of the sintered SRO ranged from approximately 0.1

to 1 μm[11]. The bulk sample quality was checked by measuring the four-terminal resistance as the temperature varied in the range 4–300 K to observe a clear kink in resistance at 163 K [see Fig. 2(b) in Ref. 2] due to the ferromagnetic transition[3,4]. For the interface resistance measurements, the pellets were cut into pieces ($\sim 3 \times 2 \times 0.5$ mm^3) and polished with sandpaper (#2000). The sample pieces were cleaned with ethanol under ultrasonication for 1 min.

Electrical interface resistances were measured by using three-terminal (3T) sensing at the interface between the sample and a conductive silver epoxy (EPO-TEK H20E, Epoxy Technology, Inc.) pad (Fig. 1). In the 3T method, one of the current lines is common to one of the voltage lines. The 3T method is therefore sensitive to the interface resistance between a sample and the common electrode, in contrast to the bulk-sensitive four-terminal method. Here we note that the $V-$ terminal of the 3T method is on the opposite side of the $I-$ terminal. Because the current does not flow between the $V+$ and $V-$ terminals (see Fig. 1), a bulk voltage drop is excluded by the 3T method. Furthermore, interface resistances for SRO-metal are significantly higher than bulk SRO resistances[2]. We therefore consider the 3T resistance as just the interface resistance of the SRO-Ag epoxy pad. In this study, we used a dc method to measure the interface resistance. A Keithley 2400 source-measure unit was used at an excitation voltage of 10 mV.

The experimental procedures were as follows. The 3T-wired SRO sample was set on a copper-plate platform with a Si-diode thermometer. Then the copper-plate platform was inserted into a cylindrical vacuum chamber surrounded by a mantle heater for regulating the temperature. The ambient air in the vacuum chamber was pumped out to a pressure of less than 1 mPa at room temperature. Measurements of the time variations of the SRO-Ag interface resistance $R(t)$ were then started. As a reducing gas, we used H_2 gas (commercial composition of purity 99.999%) or CO gas (commercial composition of purity 99.95%). The pressure of the reducing gas in the chamber was set at 50 kPa and maintained for three days. We then pumped the reducing gas out of the chamber by using a rotary pump to below $\sim$ 3 Pa in $\sim$ 5 min, and immediately substituted O_2 gas (commercial composition of purity 99.999%) at 50 kPa. We continued to measure the variations of $R(t)$ until it was almost constant. After the measurements, the procedure was repeated under different experimental conditions with the same sample. As discussed later, exposure to O_2 gas almost restored the SRO-Ag interface electrical conductivity to the initial value before exposure to

the reducing gas. We repeated a series of measurements without sample exchange. The $R(t)$ measurements were performed at temperatures from 282 to 319 K. The effects of the H_2 gas pressure was also investigated by measuring $R(t)$ at various H_2 gas pressures below 100 kPa at a constant temperature of $\simeq$ 302 K.

III. RESULTS

Figures 2 and 3 show the time variations of the normalized resistance $R(t)/R_0$ under exposure to CO (Fig. 2) or H_2 (Fig. 3) gas ($P = 50$ kPa) for $0 \leq t \leq 72$ h, and substituted O_2 ($P = 50$ kPa) for $t > 72$ h, at various temperatures. In Fig. 4, we also show the enlarged time variations of $R(t)/R_0$ around $t = 72$ h. Each R_0 value is defined as the initial resistance just before exposure to the reducing gas. CO (H_2)$\rightarrow$ O_2 denotes the process of exposure to substituted O_2 after CO (H_2) exposure. During the measurements, the temperature was regulated by a temperature controller in the presence of CO, H_2, and O_2 gas. In the CO $\rightarrow$ O_2 process, the sample temperature measured at the copper-plate platform was kept constant at all times. However, in the case of the $H_2 \rightarrow O_2$ process, the temperatures were slightly higher in the H_2 gas environment than in O_2, even when the temperature controller was set at the same temperature, because the heat-exchange efficiency of H_2 is higher than that of O_2. We therefore denote the temperatures by T_{H_2} and T_{O_2} in H_2 and O_2 atmospheres, respectively.

The figures 2 and 3 show that $R(t)/R_0$ gradually increases just after CO or H_2 exposure, and continues to increase, without reaching saturation. The rate of increase is greater at higher temperatures for both CO and H_2. The magnitude of the averaged increase rates during 72 h in H_2 is $10 - 60$ times higher than those in CO. However, the exponential behaviors in CO and H_2 are similar (this is discussed later). During pumping of CO or H_2, a small decrease in $R(t)/R_0$ (Fig. 4) was observed (this is also discussed later). After substitution of O_2 at $t = 72$ h, $R(t)/R_0$ starts to decrease rapidly and finally recovers to near the initial value, i.e., $R(t)/R_0 \approx 1$. Note that the decreases in $R(t)/R_0$ for $H_2 \rightarrow O_2$ are much faster than those for CO $\rightarrow$ O_2, i.e., the larger the increase in $R(t)/R_0$ is, the faster the decrease in $R(t)/R_0$ is.

To show the time variations precisely, we show the data for the $R(t)/R_0$ increases (R_{inc}) for CO at 307 K [Fig. 5(a)] and for H_2 at 309 K [Fig. 5(b)]. The time variations of $R(t)/R_0$

for CO fit the following function well:

$$\frac{R(t)}{R_0} = A_0 - A_1 \exp(-k_1^R t), \tag{1}$$

where A_0, A_1, and k_1^R are the fitting coefficients. In particular, k_1^R is an effective rate constant for reduction of SRO. Note that A_0 should be equal to $A_1 + 1$ in an ideal case because of a requirement of the initial condition ($R(t)/R_0 = 1$ at $t = 0$). However, we regarded A_0 as a free parameter in the data analysis. For H_2, the above function does not fit the data well, especially for temperatures higher than ~ 300 K. In the case of H_2, it is necessary to add a linear-time-dependence term:

$$\frac{R(t)}{R_0} = A_0 - A_1 \exp(-k_1^R t) + \kappa^R t, \tag{2}$$

where κ^R is a fitting coefficient. Hereafter, we use three parameters for fitting the R_{inc} data for CO (A_0, A_1, k_1^R), and four parameters ($A_0, A_1, k_1^R, \kappa^R$) for H_2. The temperature or pressure dependences of these parameters are discussed later.

Next, for analysis of the results for the $R(t)/R_0$ decrease (R_{dec}), we categorized the data into three types; (i) for CO $\rightarrow$ O_2 at lower temperatures, (ii) for CO $\rightarrow$ O_2 at higher temperatures, and (iii) for H_2 $\rightarrow$ O_2 at all temperatures, as shown in Fig. 6(a)–6(f). To clarify the time dependence, we defined O_2-time (t_{O_2}) as $t_{O_2} = 0$, at which O_2 was introduced into the chamber. Use of a logarithmic-scale plot [Fig. 6(d)–6(f)] rather than a linear-scale plot [Fig. 6(a)–6(c)] makes it easier to see the exponential decrease. Note that the R_{dec} process involves (i) one, (ii) two, or (iii) three of the exponential terms, depending on the above categorization, i.e.,

$$\frac{R(t)}{R_0} = B_0 + \sum_{n=1}^{l} B_n \exp(-k_n^O t_{O_2}), \tag{3}$$

where $B_0, B_n, k_n^O (n = 1, 2, 3)$ are fitting coefficients; k_n^O indicates an effective rate constant for oxidation of SRO, and similarly for reduction. The classification of l is as follows: (i) $l = 1$ (single exponential component) for CO $\rightarrow$ O_2 at $T < 300$ K [Fig. 6(a) and 6(d)], (ii) $l = 2$ (two exponential components) for CO $\rightarrow$ O_2 at $300 < T \leq 317$ K [Fig. 6(b) and 6(e)], and (iii) $l = 3$ (three exponential components) for H_2 $\rightarrow$ O_2 at $T \leq 319$ K [Fig. 6(c) and 6(f)]. Therefore, particularly in the case of H_2 $\rightarrow$ O_2, three time constants (fast, medium, and slow) are involved in the oxidation reaction. The difference in l is discussed later. Note

TABLE I. Effective activation energies obtained from Fig. 7 for reactions at $SrRuO_3$-Ag interface.

reducing gas	H_2	CO
E_1^R (kJ mol^{-1})	57	21
E_1^O (kJ mol^{-1})	37	55
E_2^O (kJ mol^{-1})	43	66
E_3^O (kJ mol^{-1})	57	–

that the logarithmic-scale plots in Fig. 6(d)–6(f) are expressed as $R(t)/R_0 - B_0$ for the vertical axes, where $B_0 \approx 1$.

The temperature dependences of A_0, A_1, k_1^R, and κ^R for R_{inc}, and B_0, B_n, and $k_n^O (n = 1, 2, 3)$ for R_{dec} were determining by plotting them as a function of inverse temperature, as shown in Fig. 7(a)–7(d), for R_{inc} in CO [Fig. 7(a)], for R_{dec} in CO $\rightarrow$ O_2 [Fig. 7(b)], for R_{inc} in H_2 [Fig. 7(c)], and for R_{dec} in H_2 $\rightarrow$ O_2 [Fig. 7(d)]. Note that the effective rate constants $(k_1^R, k_n^O (n = 1, 2, 3))$ strongly depend on the temperature and obey the Arrhenius equation, i.e., $k = k_0 \exp(-E_a/RT)$, where k is the rate constant, k_0 is the pre-exponential factor, E_a is the activation energy, $R = 8.31$ J mol^{-1} K^{-1} is the gas constant, and T is the temperature. Note that k_1^O for CO is connected smoothly across ~ 300 K, from which the values of k_1^O are obtained by using different fitting functions, i.e., $l = 1$ or $l = 2$ in eq.(3). This implies that the selected fitting functions are appropriate. The Arrhenius equation was used to evaluate the effective activation energies for reactions at the SRO-Ag interface; the results are shown in Table I. Each $E_1^R, E_n^O (n = 1, 2, 3)$ corresponds to the effective activation energy of $k_1^R, k_n^O (n = 1, 2, 3)$. Note that $E_n^O (n = 1, 2, 3)$ increases with increasing n; the ratio is $\frac{E_{n+1}^O}{E_n^O} \simeq 1.2 - 1.3$ (this is discussed later).

The coefficients A_0, A_1, κ^R, and $B_0, B_n (n = 1, 2, 3)$ are not strongly dependent on the temperature except for A_1, B_1, B_2 for CO. Note that the temperature variations of A_1, B_1, B_2 for CO seem to be magnified, especially on the logarithmic scale, because the reaction magnitudes for CO are much smaller than those for H_2. The reaction magnitudes for CO are therefore sufficiently small and increase with increasing temperature. In contrast, the reaction magnitudes for H_2 are relatively large and weakly dependent on temperature.

The pressure dependences of the reaction are shown by the $R(t)/R_0$ curves obtained at H_2 pressures in the range $25 - 100$ kPa at $T \simeq 302$ K in Fig. 8(a). Note that the O_2 pressure

is fixed to $P_{O_2} = 50$ kPa, as before. As shown in Fig. 8(a), R_{inc} increases with increasing H_2 pressure (P_{H_2}), and the magnitude of R_{dec} is larger after higher P_{H_2} exposure. The fitting parameters as a function of P_{H_2} are summarized for R_{inc} in H_2 at $T = 302$ K [Fig. 8(b)], and for R_{dec} in $H_2 \rightarrow O_2$ at $T = 301$ K [Fig. 8(c)]. First, for the R_{inc} process [Fig. 8(b)], the effective rate constant k_1^R hardly depends on P_{H_2}. This is reasonable because the rate constant is a function of temperature. It is important to note that the coefficient A_1 is proportional to P_{H_2} (note the linear scale on the right vertical axis), and A_0 is nearly equal to $A_1 + 1$. Furthermore, the linear-time-dependence term κ^R also shows P_{H_2} dependence, i.e., the higher P_{H_2} is, the larger κ^R is. The origins of the pressure dependences are discussed later. For the R_{dec} process [Fig. 8(c)], similarly to the case for the R_{inc} process, the effective rate constants $k_n^O (n = 1, 2, 3)$ are independent of P_{H_2}; this is reasonable, as discussed above. In addition, the coefficients $B_n (n = 1, 2, 3)$ are nearly proportional to P_{H_2} (note the linear scale on the right vertical axis); this is discussed later.

IV. DISCUSSION

We now discuss the mechanism of R_{inc} during reducing gas (CO, H_2) exposure, and R_{dec} during O_2 gas exposure. The time variation functions used above to fit the $R(t)/R_0$ data can be explained in terms of oxygen deficiency. In a reducing gas environment, oxygen atoms near the surface/interface are expected to leave the surface/interface through a reduction process, even at room temperature[12]. In contrast, in an O_2 gas environment, oxygen vacancies are filled with oxygen atoms again through the oxidation process. Figure 9(a) shows schematically that an oxygen atom at the SRO surface/interface recombines with a H_2 molecule that is approaching the surface/interface. As shown in previous studies[13], oxygen deficiency results in low electrical conductivity. Thus, $R(t)/R_0$ at the SRO-Ag interface is expected to increase in a reducing environment, as previously reported[2]. We assume that the generation of oxygen vacancies in SRO occurs as follows: $SrRuO_3 + xCO \rightarrow SrRuO_{3-x} + xCO_2$, or $SrRuO_3 + xH_2 \rightarrow SrRuO_{3-x} + xH_2O$. Here, we consider the reactions to be pseudo-first-order reactions if the reducing gas contents are kept constant because excess reducing gas was used in the experiments. We therefore consider that the reactions depend only on the oxygen contents at the surface/interface. The oxygen-deficient process can

therefore simply be described by the following rate equation[14]:

$$-\frac{d(C_0 - x(t))}{dt} = k_1^R(C_0 - x(t)), \tag{4}$$

where C_0 is the initial content of oxygen around the silver epoxy pad at the surface/interface, $x(t)$ is the number of oxygen vacancies at time t, and k_1^R is the effective rate constant for the reduction. Therefore $C_0 - x(t)$ represents the oxygen content around the pad at time t.

By solving differential eq.(4), we obtain $x(t) = C_0[1 - \exp(-k_1^R t)]$. Assuming that the surface/interface resistance change ΔR is proportional to the number of oxygen vacancies $x(t)$,

$$\frac{\Delta R}{R_0} = \frac{R(t) - R_0}{R_0} = \frac{R(t)}{R_0} - 1 = \alpha x(t), \tag{5}$$

where α is not a simple constant but a type of function without the variable $x(t)$. The fitting function for $R(t)/R_0$ for reduction is derived as follows:

$$\begin{aligned}\frac{R(t)}{R_0} &= 1 + \alpha x(t) = 1 + \alpha C_0 - \alpha C_0 \exp(-k_1^R t) \\ &= A_0 - A_1 \exp(-k_1^R t),\end{aligned} \tag{6}$$

where $A_0 = A_1 + 1$ and $A_1 = \alpha C_0$. As A_1 is proportional to P_{H_2} in Fig. 8(b), α is proportional to P_{H_2}. Here, we consider that α has a physical meaning and refers to the collision frequency of the reducing gas with the surface/interface because a larger α should lead to a larger $\frac{\Delta R}{R_0}$ (note that α is a dimensionless parameter in this study). The collision frequency z of gas molecules attacking the surface is expressed as $z = \frac{P}{\sqrt{2\pi m k_B T}}$, where P is the gas pressure, m is the mass of a gas molecule, k_B is the Boltzmann constant, and T is the temperature[15]. Therefore, taking m into account, the ratio of z for CO and H_2 at a certain temperature and pressure is calculated as $\frac{z_{H_2}}{z_{CO}} \simeq 3.7$. The value is close to the ratio $\frac{A_1(H_2)}{A_1(CO)} \sim 3.8$ at ~ 318 K. This confirms that the fitting function of eq.(6) is reasonable. Note that the ratio $\frac{A_1(H_2)}{A_1(CO)}$ at low temperatures is apparently larger than 3.7 (~ 17 at ~ 291 K, ~ 13 at ~ 300 K, and ~ 9 at ~ 308 K). Presumably because A_1 is too small for CO in the early stage of the reaction at low temperatures compared with that for H_2, the ratio $\frac{A_1(H_2)}{A_1(CO)}$ seems to be large.

However, the additional term in the experimental linear-time-dependence $\kappa^R t$ under H_2 exposure is not explained by only eq.(6). The origin of the linear term might not be the simple oxygen deficiency described above. We propose that a possible origin is a secondary reaction at the SRO surface/interface with generated H_2O because the $\kappa^R t$ term is necessary to fit the data only for H_2, not for CO. For example, a reaction such as $SrO + H_2O \rightarrow Sr(OH)_2$

would disturb the surface/interface SRO atomic rows[7], which would increase $R(t)/R_0$. The other possibility is that the generated H_2O is incorporated into the SRO-Ag interface. For example, the resistances of oxide films (TiO_x[16] and Al-doped ZnO[17,18]) containing grain boundaries change in a high-humidity environment. At present, the origin of the linear term $\kappa^R t$ is unclear. However, the above scenarios are experimentally consistent with the pressure dependence of κ^R, i.e., a higher κ^R at a higher P_{H_2} [Fig. 8(b)], because H_2O generation would increase with increasing P_{H_2}. Here, we regard the amount of residual H_2O (not generated H_2O) left in the experimental apparatus, i.e., from gas bottles and gas lines, as trivial because $R(t)/R_0$ was almost kept constant with time before exposure to reducing gas in each experimental run [see Fig. 2 and 3].

In contrast, the oxidation process under O_2 exposure, as seen in Fig. 9(b), can be described by the following differential equation, similarly to the R_{inc} process:

$$\frac{d(C_0 - x(t))}{dt} = k_1^O x(t), \tag{7}$$

where C_0 and $x(t)$ are the same as in eq.(4), and k_1^O is the effective rate constant for oxidation. By solving eq.(7), we obtain $x(t) = x_0 \exp(-k_1^O t_{O_2})$, where x_0 is the initial number of oxygen vacancies at $t_{O_2} = 0$. Similarly to eqs.(5) and (6),

$$\begin{aligned}\frac{R(t)}{R_0} &= 1 + \alpha_1' x(t) = 1 + \alpha_1' x_0 \exp(-k_1^O t_{O_2}) \\ &= B_0 + B_1 \exp(-k_1^O t_{O_2}),\end{aligned} \tag{8}$$

where α_1' is similar to α, $B_0 = 1$, and $B_1 = \alpha_1' x_0$. The simple form, i.e., eq.(8), explains the single-exponential process ($l = 1$) for R_{dec} of $CO \rightarrow O_2$ at low temperatures when $\Delta R/R_0 < 5\%$. As seen in Fig. 8(c), B_1 is proportional to P_{H_2}, which means that x_0 is proportional to P_{H_2}. It is reasonable to suppose that the initial number of oxygen vacancies x_0 (at $t_{O_2} = 0$) should be proportional to P_{H_2} (as discussed above). Here, α_1' would be proportional to P_{O_2} by analogy with α for P_{H_2}. However, we consider α_1' to be constant in this experiment because P_{O_2} is fixed at 50 kPa. Figure 8(c) shows that the coefficients B_2 and B_3 are also proportional to P_{H_2}, which suggests that B_2 and B_3 are also proportional to x_0. We therefore assume that the processes with two or three exponential components ($l = 2, 3$) are based on the same mechanism as that for $l = 1$. We consider that each exponential term $\exp(-k_n^O t_{O_2})(n = 1, 2, 3)$ corresponds to a different oxidation rate, i.e., k_1^O, k_2^O, and k_3^O correspond to slow, medium, and fast rate constants, respectively. Each

coefficient (B_1, B_2, B_3) and each effective activation energy $(E_1^O,\ E_2^O,\ E_3^O)$ also correspond to slow, medium, and fast oxidation processes, respectively. These deductions show that reactions with different rates occur in parallel. Recall that only a single or two exponential components are necessary for the oxidation of CO $\rightarrow$ O_2, whereas at least three components are necessary for H_2 $\rightarrow$ O_2, which reflects the magnitudes of $\Delta R/R_0$. The larger $\Delta R/R_0$ implies that the oxygen deficiency spreads not only just below the surface/interface but also deeper into the subsurfaces.

Here, we simply assume that the rate constants k_1^O, k_2^O, k_3^O, which differ approximately tenfold, correspond to the reaction at the topmost surface/interface, the second-top one, and the third-top one, respectively [Fig. 9(c)]. We note that Fig. 9 is a solely speculative picture in which we show the different rate constants depending on the depth below the surface/interface. This model is supported by the order of the magnitudes of the effective activation energies (Table I). For example, E_1^O is naturally the smallest among the E_n^O values because the reactivity should be highest at the surface/interface. E_2^O is 1.2 times larger than E_1^O, and E_3^O is 1.3 times larger than E_2^O. This suggests that the effective activation energy increases from the surface/interface to subsurfaces deeper inside the bulk. The reactivity inside the SRO away from the surface/interface should be strongly temperature dependent because a higher temperatures considerably accelerates the inside reactions. We therefore consider that E_1^O, E_2^O, and E_3^O correspond to the effective activation energies at the topmost surface/interface, the second-top one, and the third-top one, respectively. In terms of the order of the rate-constant magnitudes, i.e., $k_3^O > k_2^O > k_1^O$, stronger forces would yield larger rate constants. Because oxygen deficiency must be energetically more unstable inside the bulk than at the topmost surface, replenishing oxygen atoms at the deficiency sites at the deeper subsurfaces would yield stronger forces. The magnitudes of the coefficients $B_n (n = 1, 2, 3)$ are not equal but $B_3 > B_2 > B_1$, as shown in Fig. 8(c). Considering $B_n = \alpha_n' x_0$, similarly to eq.(8), the difference in B_n indicates the difference in α_n' or x_0. Generally, the oxygen deficiency x_0 at a layer deeper than the surface/interface should be less than that near the surface/interface. However, The B_n order indicates the opposite trend. We therefore suppose that α_n' indicates that oxygen atom adsorption is strongly layer dependent, which shows that α_n' increases with increasing n. In other words, the probability of oxygen atoms replenishing deficiency sites in deeper layers is higher than that of sites at the surface/interface being filled. Note that the order $B_3 > B_2 > B_1$ is consistent with the

data shown in Fig. 7(d) at the same pressure, i.e., $P_{O_2} = 50$ kPa. In this work, we considered multicomponent k_n^O processes up to $n = 3$. However, numbers higher than $n = 3$ would be necessary if the oxygen deficiency expanded into deeper layers from the surface/interface, with larger $\Delta R/R_0$.

Here, we reiterate that $R(t)/R_0$ decreases even during the pumping of the reducing gas before O_2 is substituted (Fig. 4). The magnitude of $\Delta R/R_0$ is small for the entire resistance decrease. However, it is larger than the value expected from the temperature decrease ($1-2$ K) due to pumping out of the thermal exchange gas. The magnitude of $\Delta R/R_0$ due to the temperature change is estimated to be 1.1×10^{-3}/K above 163 K from Fig. 2(d) in Ref. 2. This implies that pumping reducing gas also contributes to the refilling of oxygen vacancy sites. If some intermediate reduction states such as water-like species of O-H_2[19] adsorb on the SRO-Ag interface, pumping reducing gas may cause some of the reverse process, i.e., oxygen atoms going back to the vacancy sites. Furthermore, when H_2 is used for reduction, the generated H_2O may be incorporated onto the SRO-Ag interface and contribute to R_{inc}, as mentioned before. Thus, part of R_{dec} during H_2 pumping may include the H_2O evacuation effect. As seen in Fig. 4, however, we stress that the major origin of R_{dec} is O_2 exposure in this experiment. The interface resistance decreases to almost the initial value, i.e., that before exposure to a reducing gas, probably because oxygen vacancies are forced to refill with oxygen atoms under O_2 exposure.

We note that the temperature dependence of the 3T resistance exhibited metallic behavior after exposure to the reducing gas, as well as before exposure [see Figs. 2(d) in Ref. 2 and S1 in the supplementary material]. Oxygen vacancies generated by reducing gas exposure could act as lattice defects in the metallic states, causing increased interface resistance. However, we also note that additional defects may play a role in the $R(t)/R_0$ variation because the surface composition of SRO was not evaluated by surface-sensitive measurements except for the 3T resistance measurements.

In summary, for the R_{inc} process, oxygen deficiency progresses gradually with a single exponential component for both CO and H_2, except for the linear-time-dependence term. A single exponential component means that reduction occurs successively from the top surface/interface to the subsurfaces. The linear-time-dependence term might be related to a secondary reaction and/or incorporation of H_2O into the interface. Exposure to CO generates low oxygen deficiency at room temperature, whereas H_2 causes high oxygen deficiency.

Single or multiple exponential components appear in the R_{dec} process and reflect the degree of oxygen deficiency. A single exponential component is sufficient for CO $\rightarrow$ O_2 at $T < 300$ K, but at least three exponential components are necessary for H_2 $\rightarrow$ O_2. In the R_{dec} process, oxygen atoms are adsorbed at deficiency sites, with the fastest rate at the deeper sites below subsurfaces, and the slowest rate at the topmost surface/interface sites. Future work will seek to clarify the depth dependence in the SRO redox reaction by direct measurement via *in situ* secondary ion mass spectrometry.

V. CONCLUSIONS

A three-terminal method was used for interface-sensitive measurements of electrical resistance, we studied the time variations of reducing and oxidation reactions at a $SrRuO_3$-silver epoxy interface on exposure to CO, H_2, and O_2 gas at room temperature. The reducing process can be described as a pseudo-first-order reaction that causes oxygen deficiency, and this increases the interface resistance with a single exponential component. By extension, the oxidation process can also be explained by a similar model, in which oxygen atoms are adsorbed near the surface/interface in multiple ways. This shows that the interface resistance decreases for multiple exponential components. In this work, we showed that interface-sensitive resistance measurements provide a good sensing method for detecting reaction precursors at the interfaces of conducting materials.

SUPPLEMENTARY MATERIAL

See the supplementary material for the temperature dependence of the 3T resistance before and after H_2 gas exposure.

ACKNOWLEDGMENTS

The authors are grateful to F. Ito for useful comments. This work was supported by JSPS KAKENHI Grant Number JP19K03743. We thank Helen McPherson, PhD, from Edanz (https://jp.edanz.com/ac) for editing a draft of this manuscript.

AUTHOR DECLARATIONS

Conflict of Interest

The authors have no conflicts to disclose.

AUTHOR CONTRIBUTIONS

H. K.: Conceptualization (lead); Methodology (equal); Data curation (equal); Writing-original draft (lead); Writing-review & editing (equal). H. S.: Methodology (equal); Data curation (equal). K. T.: Methodology (equal); Writing-review & editing (equal).

DATA AVAILABILITY

The data that support the findings of this study are available from the corresponding author upon reasonable request.

REFERENCES

[1]D. Spreitzer, and J. Schenk, Steel Research Int. **90**, 1900108 (2019).

[2]H. Kambara, H. Tanaka, S. Oishi, K. Tenya, and H. Tsujii, J. Appl. Phys. **128**, 175306 (2020).

[3]P. B. Allen, H. Berger, O. Chauvet, L. Forro, T. Jarlborg, A. Junod, B. Revaz, and G. Santi, Phys. Rev. B **53**, 4393 (1996).

[4]G. Koster, L. Klein, W. Siemons, G. Rijnders, J. S. Dodge, C.-B. Eom, D. H. A. Blank, and M. R. Beasley, Rev. Mod. Phys. **84**, 253 (2012).

[5]W. Bensch, H. W. Schmalle, and A. Reller, Sol. Sta. Ion. **43**, 171 (1990).

[6]J. Lin, K. Natori, Y. Fukuzumi, M. Izuha, K. Tsunoda, K. Eguchi, K. Hieda, and D. Matsunaga, Appl. Phys. Lett. **76**, 2430 (2000).

[7]J. Lin, K. Tsunoda, K. Eguchi, K. Hieda, and D. Matsunaga, J. Vac. Sci. Technol. A **20**, 84 (2002).

[8]D. Halley, C. Rossel, D. Widmer, H. Wolf, and S. Gariglio, Mat. Sci. Eng. B **109**, 113 (2004).

[9]H. N. Lee, H. M. Christen, M. F. Chisholm, C. M. Rouleau, and D. H. Lowndes, Appl. Phys. Lett. **84**, 4107 (2004).

[10]M. Mlynarczyk, K. Szot, A. Petraru, U. Poppe, U. Breuer, R. Waser, and K. Tomala, J. Appl. Phys. **101**, 023701 (2007).

[11]H. Kambara, Y. Obinata, K. Tenya, and H. Tsujii, Jpn. J. Appl. Phys. **55**, 093004 (2016).

[12]H. Over, Chem. Rev. **112**, 3356 (2012).

[13]M. Hiratani, C. Okazaki, K. Imagawa, and K. Takagi, Jpn. J. Appl. Phys. **35**, 6212 (1996).

[14]P. Atkins, J. de Paula, and J. Keeler, *Atkins' Physical Chemistry, Eleventh ed.* (Oxford University Press, 2018) Focus 17.

[15]P. Atkins, J. de Paula, and J. Keeler, *Atkins' Physical Chemistry, Eleventh ed.* (Oxford University Press, 2018) Focus 16.

[16]G. Zhou, S. Duan, P. Li, B. Sun, B. Wu, Y. Yao, X. Yang, J. Han, J. Wu, G. Wang, L. Liao, C. Lin, W. Hu, C. Xu, D. Liu, T. Chen, L. Chen, A. Zhou, and Q. Song, Adv. Electron. Mater. **4**, 1700567 (2018).

[17]T. Miyata, Y. Ohtani, T. Kuboi, and T. Minami, Thin Solid Films **516**, 1354 (2008).

[18]T. L. Chen, D. S. Ghosh, D. Krautz, S. Cheylan, and V. Pruneri, Appl. Phys. Lett. **99**, 093302 (2011).

[19]Q. Sun, K. Reuter, and M. Scheffler, Phys. Rev. B **70**, 235402 (2004).

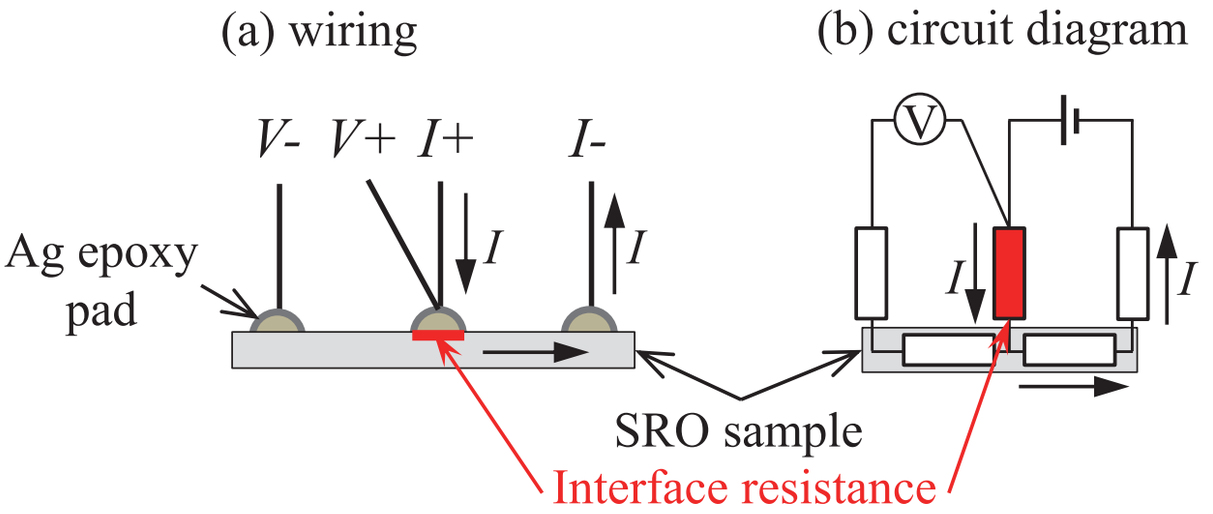

FIG. 1. Schematics of (a) wiring and (b) circuit diagram of the electrical resistance measurement for three-terminal (3T) method. Interface resistance marked in red is measured.

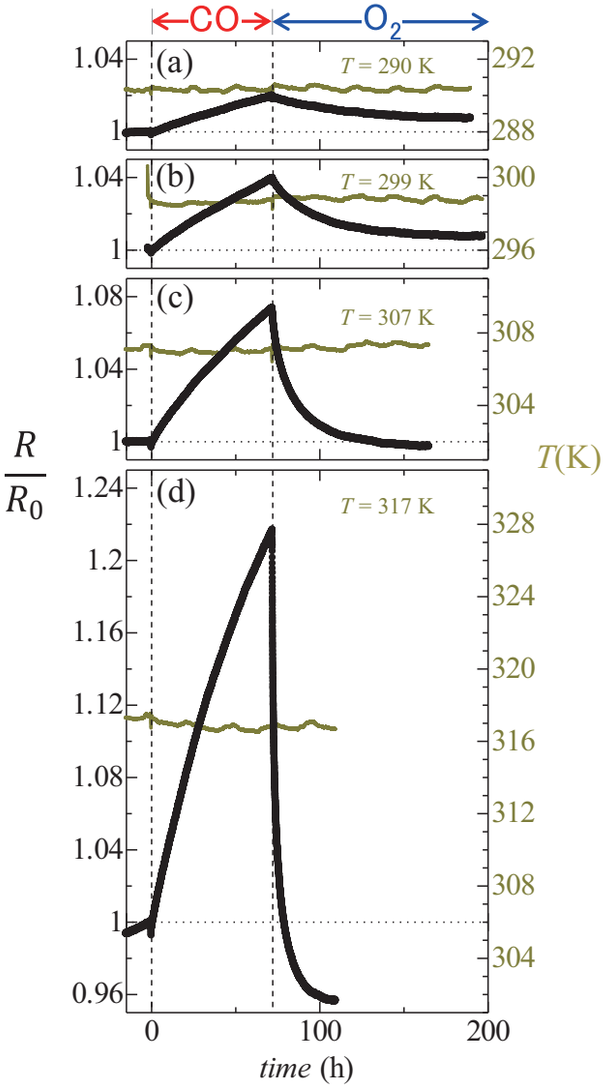

FIG. 2. Time variations of normalized resistances $R(t)/R_0$ of $SrRuO_3$-Ag in CO and O_2 gas atmospheres (50 kPa of CO at $0 \leq t \leq 72$ h, and 50 kPa of O_2 at $t \geq 72$ h) at fixed temperatures: (a) 290 K, (b) 299 K, (c) 307 K, and (d) 317 K. Right vertical axes denote temperatures.

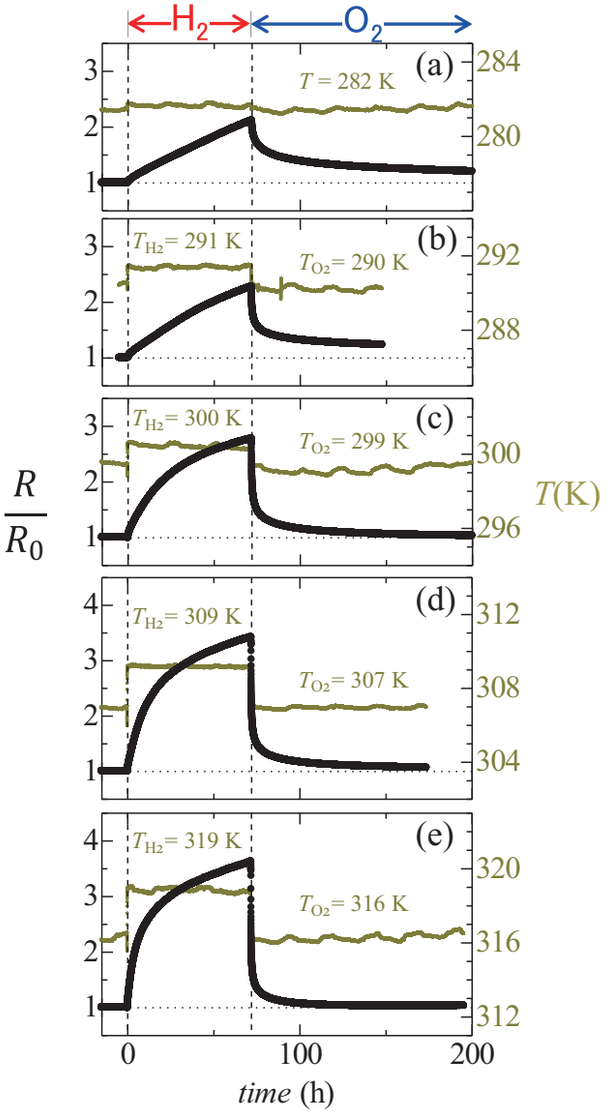

FIG. 3. Time variations of normalized resistances $R(t)/R_0$ of $SrRuO_3$-Ag in H_2 and O_2 gas atmospheres (50 kPa of H_2 at $0 \leq t \leq 72$ h, and 50 kPa of O_2 at $t \geq 72$ h) at fixed temperatures. T_{H_2} (T_{O_2}) denote the temperatures in H_2 (O_2) gas atmospheres (T_{H_2} are slightly higher than T_{O_2}, as discussed in the text). Right vertical axes denote temperatures.

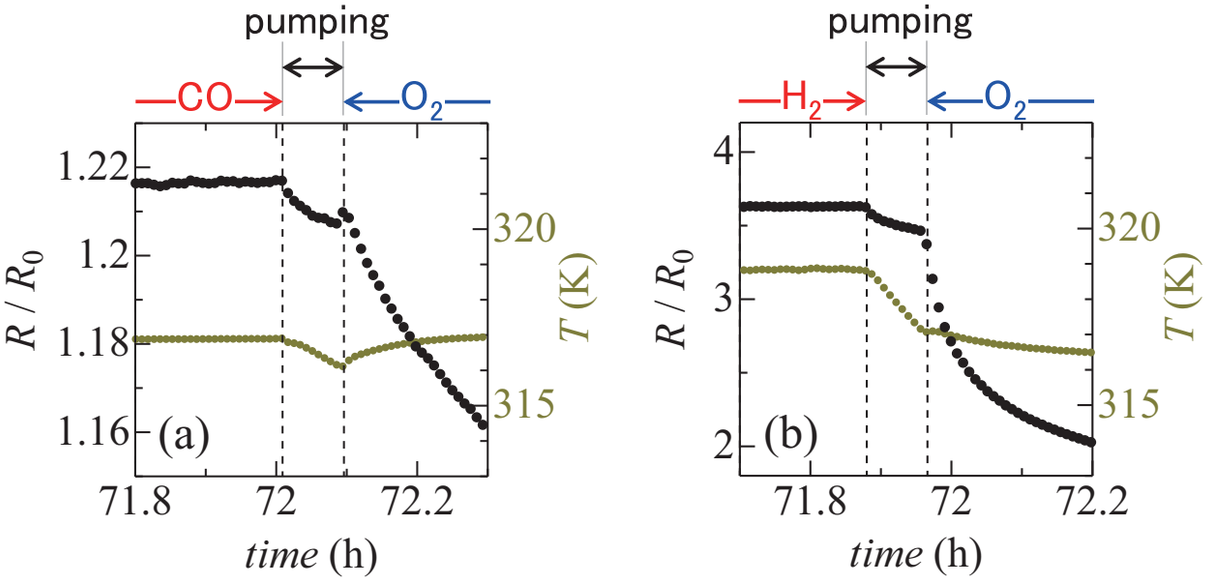

FIG. 4. Examples of the enlarged time variations of $R(t)/R_0$ around $t = 72$ h for (a) CO $\rightarrow$ O_2 at 317 K (corresponding to Fig. 2(d)), and (b) H_2 $\rightarrow$ O_2 at $T_{H_2} = 319$ K ($T_{O_2} = 316$ K) (corresponding to Fig. 3 (e)). Right vertical axes denote temperatures.

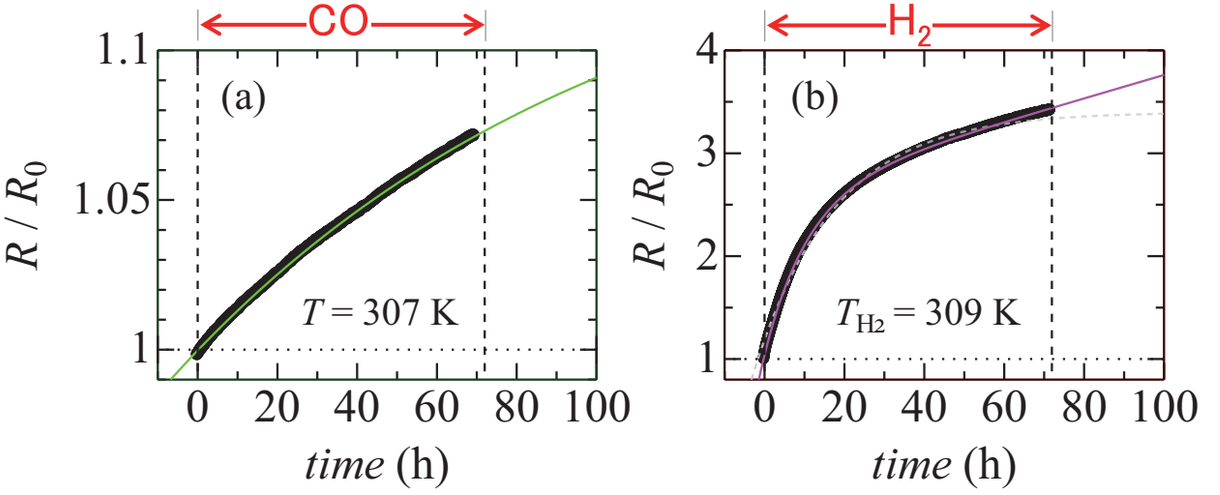

FIG. 5. Examples of R_{inc} data analyses. $R(t)/R_0$ vs time in CO at 307 K (a) and H_2 at 309 K (b). Thin solid curves denote fits using eq.(1) in (a) and eq.(2) in (b). Dashed curve in (b) is fit using eq.(1), for reference.

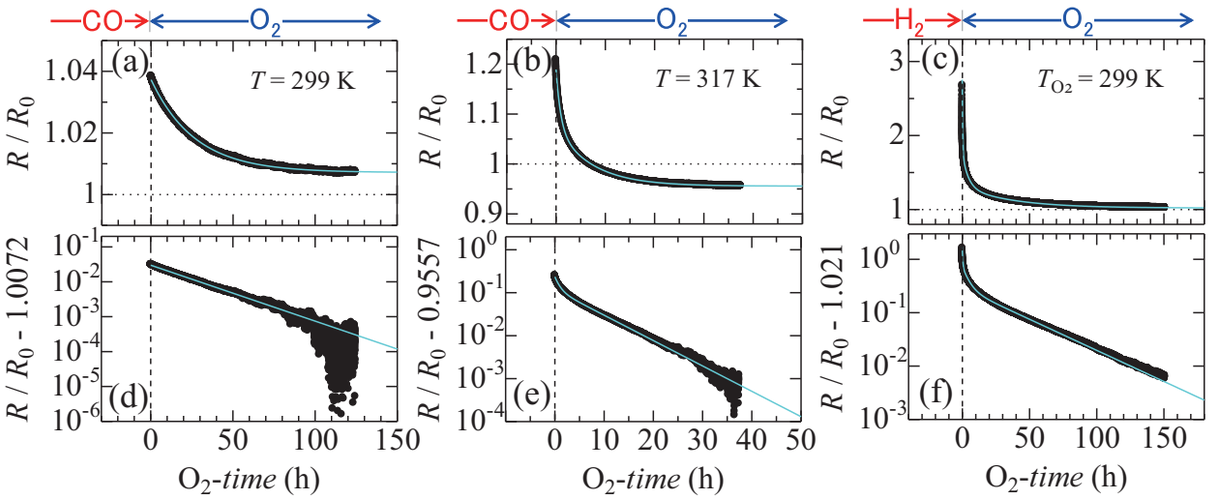

FIG. 6. Examples of R_{dec} data analyses. $R(t)/R_0$ vs time in CO → O_2 at 299 K (a, d), CO → O_2 at 317 K (b, e), and H_2 → O_2 at 299 K (c, f): (a–c) linear-scale plots, (d–f) logarithmic-scale plots after subtraction of B_0 values. Thin solid curves are fits obtained using eq.(3).

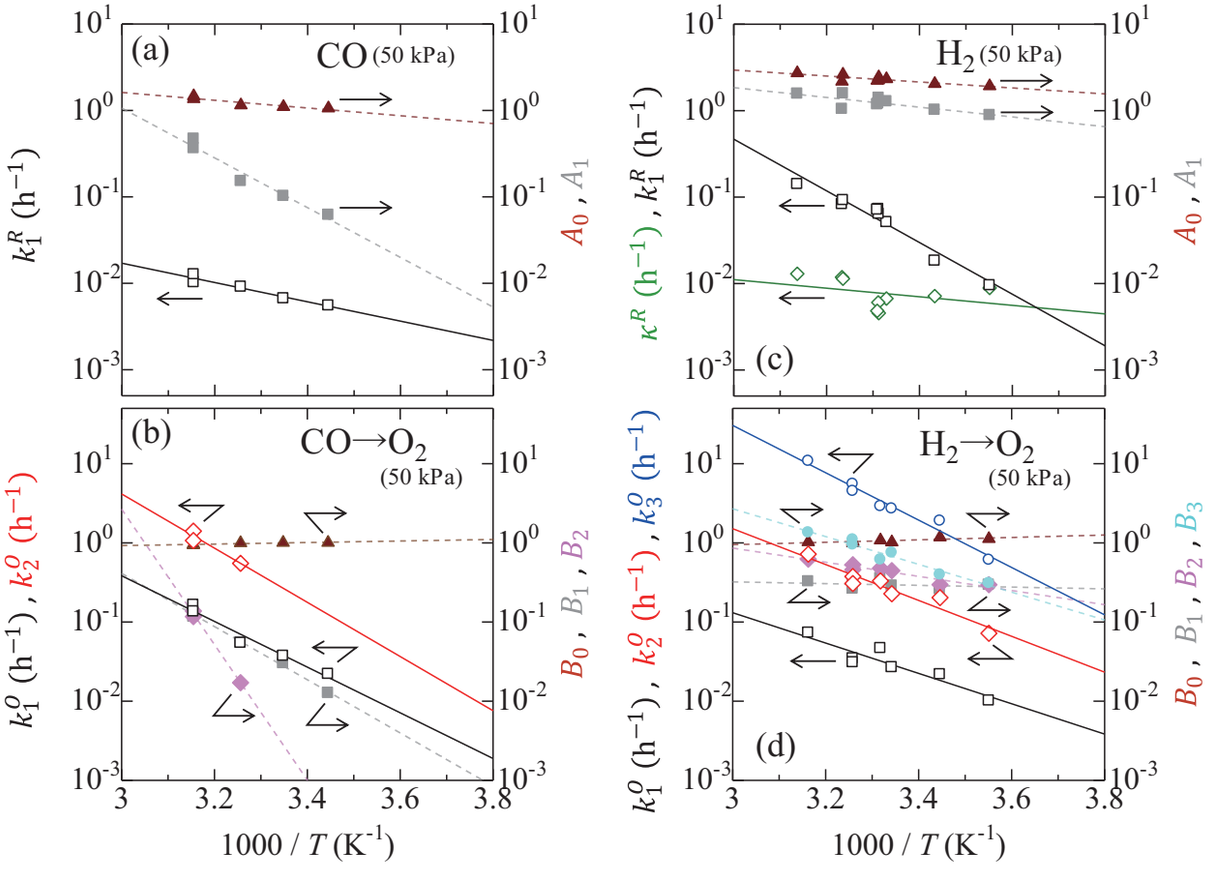

FIG. 7. Rate constants ($k_1^R, k_1^O, k_2^O, k_3^O$), t-linear term κ^R (left vertical axes) and fitting coefficients ($A_0, A_1, B_0, B_1, B_2, B_3$) (right vertical axes) vs inverse temperature: (a) R_{inc} in CO, (b) R_{dec} in CO $\rightarrow$ O_2, (c) R_{inc} in H_2, and (d) R_{dec} in H_2 $\rightarrow$ O_2.

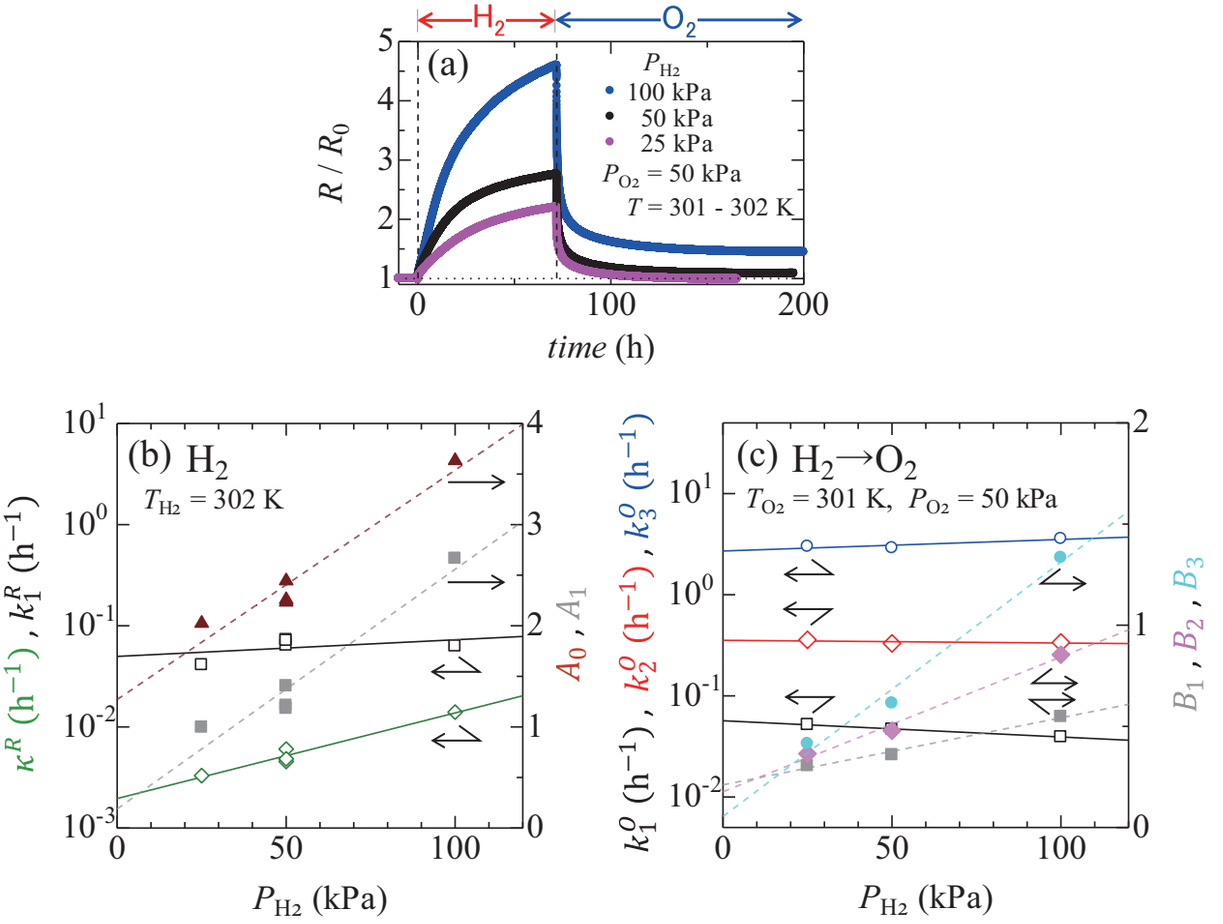

FIG. 8. H_2 pressure (P_{H_2}) dependence at 301–302 K of (a) $R(t)/R_0$ vs time, (b) k_1^R, κ^R (left vertical axis), A_0, A_1 (right vertical axis) vs P_{H_2} for R_{inc}, and (c) k_1^O, k_2^O, k_3^O (left vertical axis), B_1, B_2, B_3 (right vertical axis) vs P_{H_2} for R_{dec}. Note that O_2 pressure is fixed at $P_{O_2} = 50$ kPa.

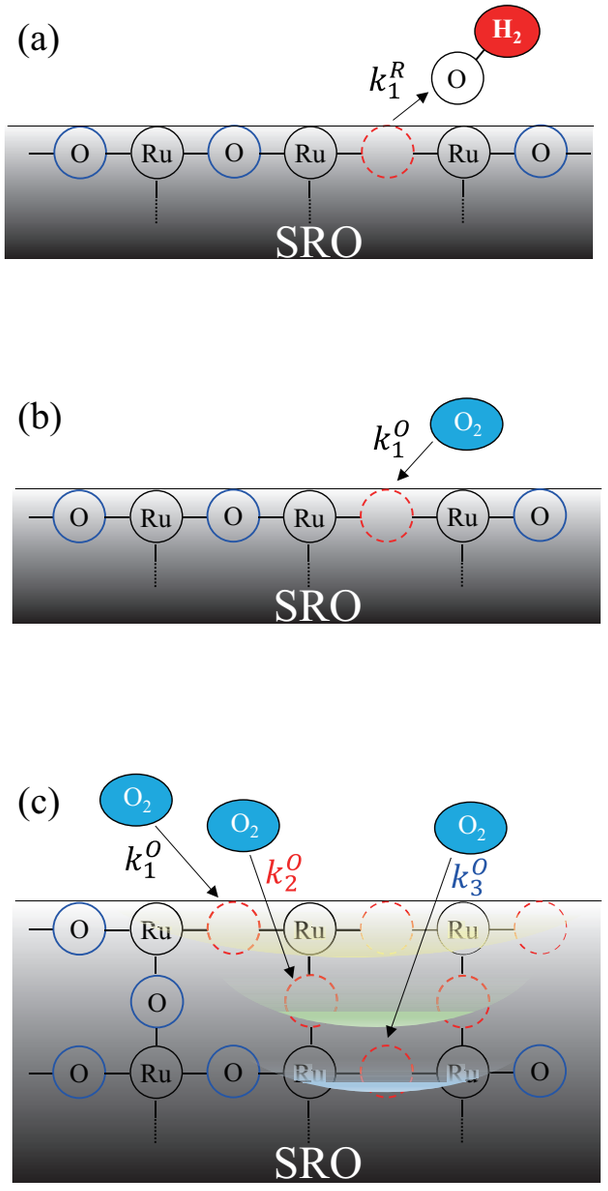

FIG. 9. Schematic diagrams of reactions at topmost surface/interface of $SrRuO_3$ in (a) H_2 atmosphere, with rate constant k_1^R, and (b) O_2 atmosphere, with rate constant k_1^O. (c) When the degree of oxygen deficiency is high (not only at the topmost surface/interface but also deeper subsurfaces), not only k_1^O but also faster rate constants (k_2^O and k_3^O) appear in an O_2 atmosphere.

Journal of Applied Physics

AIP Publishing

Journal of Applied Physics

AIP Publishing

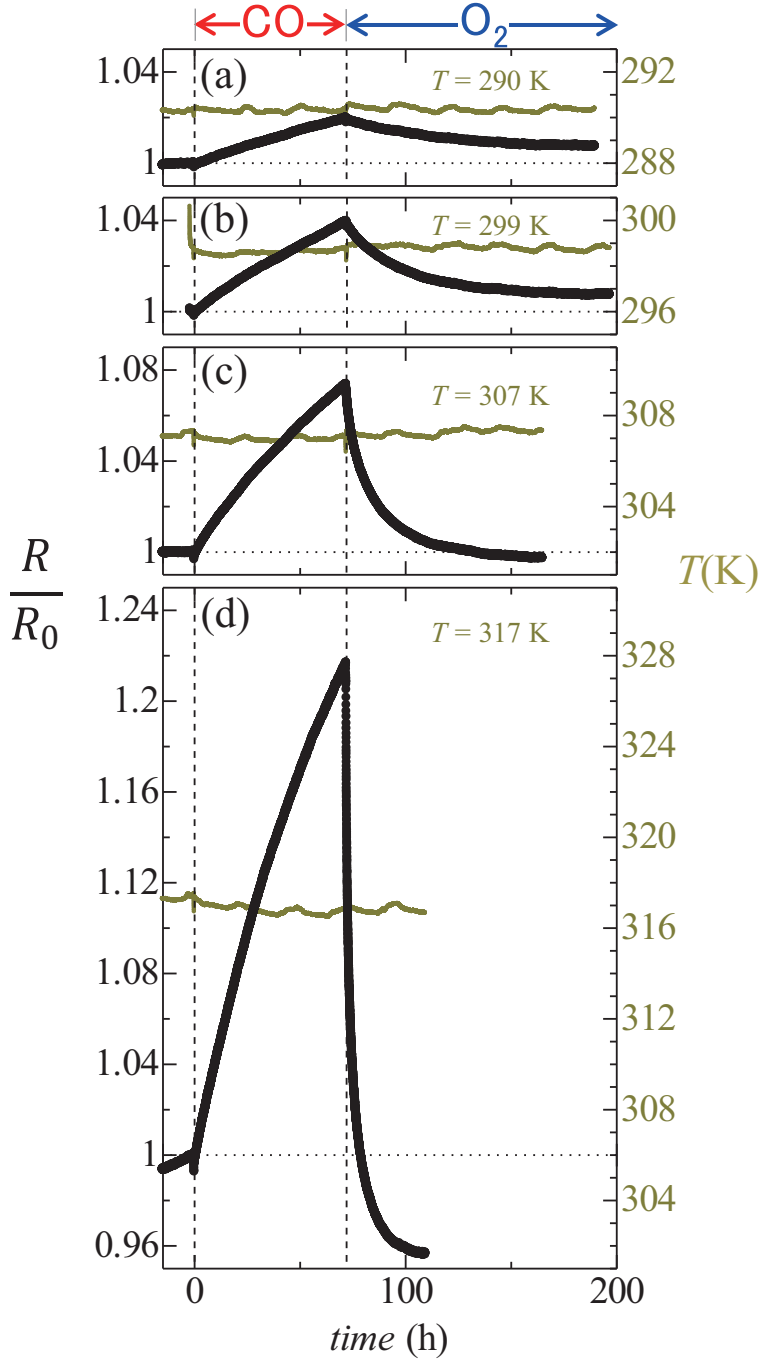

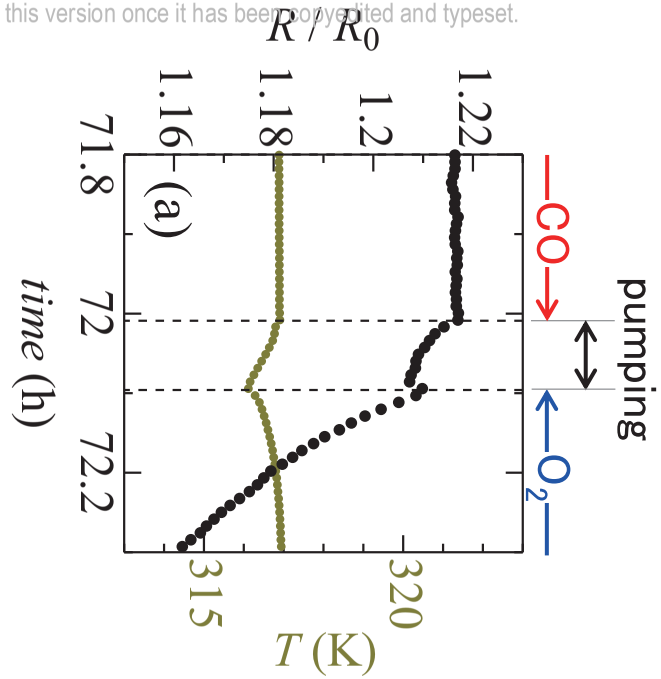

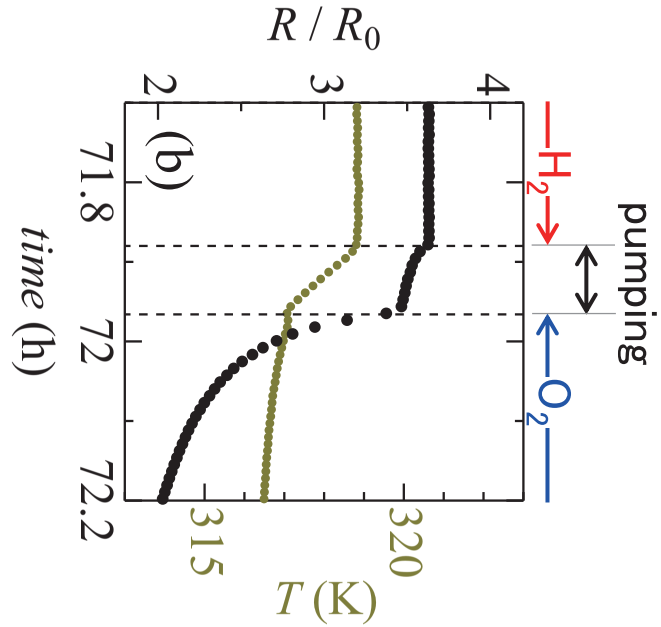

AIP Publishing

Journal of Applied Physics

PLEASE CITE THIS ARTICLE AS DOI: 10.1063/5.0135695

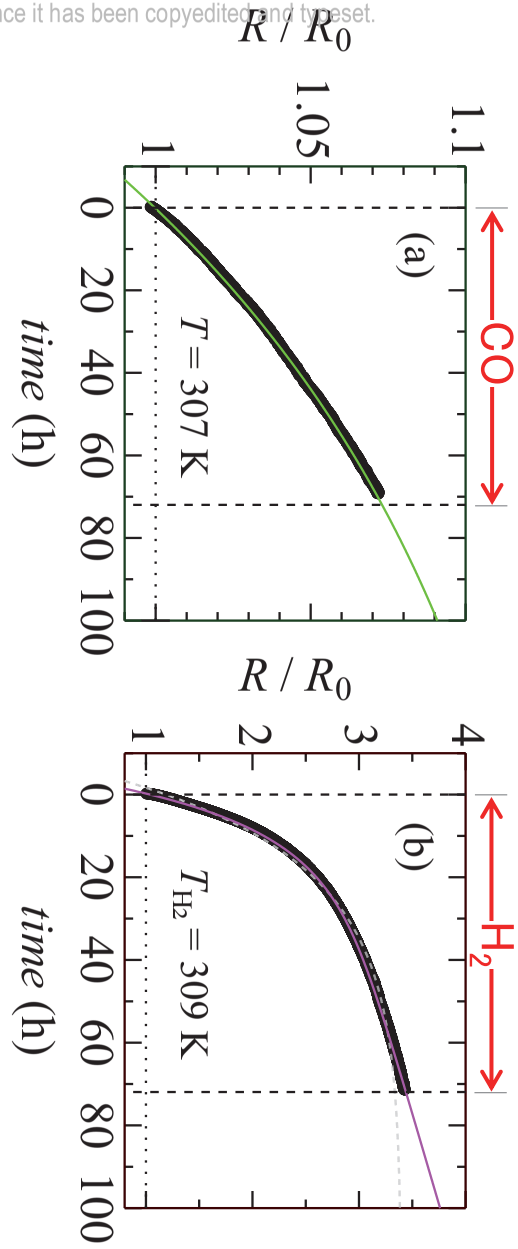

Journal of Applied Physics

AIP Publishing

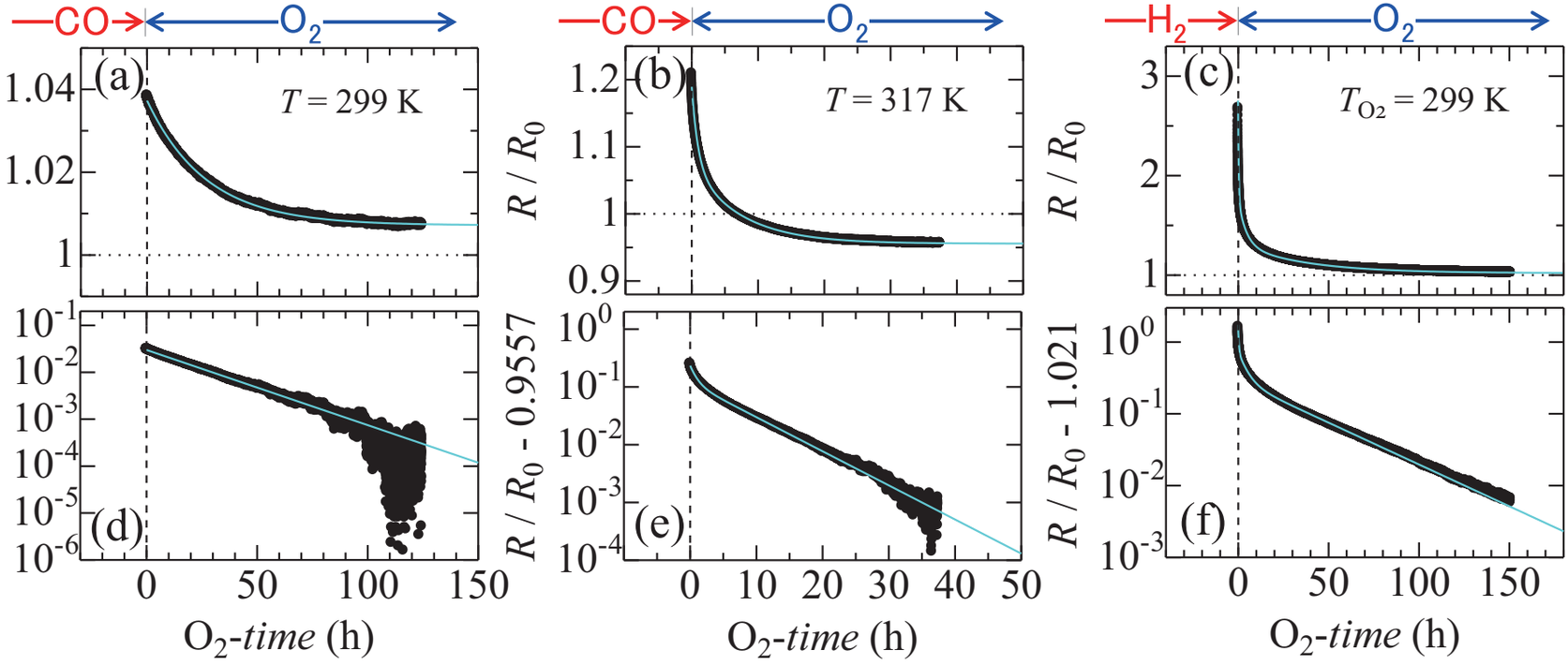

AIP Publishing
Journal of Applied Physics
ACCEPTED MANUSCRIPT